

# Interpretable Latent Spaces for Learning from Demonstration

**Yordan Hristov**  
University of Edinburgh  
yordan.hristov@ed.ac.uk

**Alex Lascarides**  
University of Edinburgh  
alex@inf.ed.ac.uk

**Subramanian Ramamoorthy**  
University of Edinburgh  
sramamoo@inf.ed.ac.uk

**Abstract:** Effective human-robot interaction, such as in robot learning from human demonstration, requires the learning agent to be able to ground abstract concepts (such as those contained within instructions) in a corresponding high-dimensional sensory input stream from the world. Models such as deep neural networks, with high capacity through their large parameter spaces, can be used to compress the high-dimensional sensory data to lower dimensional representations. These low-dimensional representations facilitate symbol grounding, but may not guarantee that the representation would be human-interpretable. We propose a method which utilises the grouping of user-defined symbols and their corresponding sensory observations in order to align the learnt compressed latent representation with the semantic notions contained in the abstract labels. We demonstrate this through experiments with both simulated and real-world object data, showing that such alignment can be achieved in a process of physical symbol grounding.

**Keywords:** grounded language acquisition, disentanglement learning, symbol grounding

## 1 Introduction

We want our autonomous robots to be competent across broad domains. Ideally, the robot must be able to cope with the open world, i.e., one where it may not be possible to provide a complete specification of the task up front. This makes it important for the robotic agent to incrementally learn about the world and its regularities in order to be able to efficiently generalize to new situations. It can be argued that such generalizations are made easier when the models used by the robot can represent concepts ranging from object-ness to causal relationships.

Learning from human demonstration [1, 2] is an efficient way to transfer such knowledge to a robot, wherein the human expert teaches a robot by showing it instances of execution of the task of interest. There are numerous examples of fairly sophisticated behaviours being taught to robots, such as control and planning in high dimensional systems [3, 4, 5]. A common theme across a majority of these works is that the target of transfer is the behaviour so that the robot is taught to mimic the motion (with learning methods being used to generalise over, say, differing body configurations). We are also interested in being able to transfer other aspects of knowledge about the world which may allow the robot to infer deeper concepts. A necessary first step towards this form of teaching or transfer is to give the robotic agent the ability to learn models that represent structure in ways that are similar to corresponding human notions - so that it may be possible for the human expert and robot to leverage common grounding [6].

From a different direction, there is recognition among roboticists that models and policies used by autonomous robotic agents should be explainable [7, 8]. The notion of what it means to interpret and explain is in itself a topic of active debate at the moment but we believe it is safe to argue that grounded models used by robots should satisfy key desiderata. For instance, the notion of similarity with which items are grouped together must align with corresponding human notions or that factors

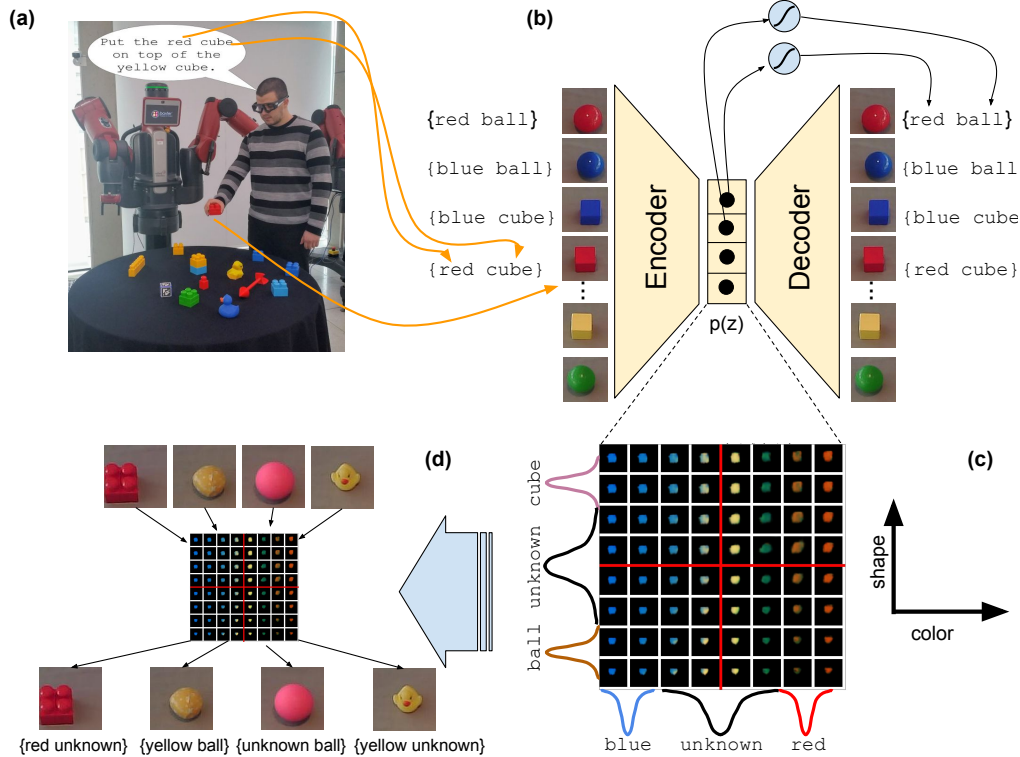


Figure 1: Overview of the full framework. The expert is demonstrating the task at hand while uttering symbols which are grounded according to their attention in the environment. The conceptual grouping of the symbols is given. **(a)** The gathered dataset is used to train a variational auto-encoder with a set of auxiliary classification losses - one per conceptual group. Each classifier takes information from a single latent dimension. **(b)** The training procedure guarantees that the semantic meaning of each group will be encoded in a separate latent dimension with linearly separable classes **(c)** Using the per-class estimated 1D Normal distributions, together with in-between distributions for unknown labels, we can perform KNN classification

of variation implied by the model should be understandable to a human expert. These desiderata are closely aligned with the emerging literature on learning disentangled representations.

In this paper, we focus on learning models of objects of the kind that robots might encounter in manipulation settings. In order to make the underlying concepts fully clear, we use simple objects that uncontroversially expose the structure of the domain. For instance, we show that after being exposed only to a few instances of a ball and a cube, the agent can figure out that other instances of cubes can be labelled as such (without this fact being explicitly stated by the expert).

Our main contribution consists of a framework—see Figure 1—which allows for independent user-defined factors of variation, manifested in a high-dimensional space, to be projected to a lower-dimensional latent space, by preserving the factors’ orthogonality. The latter is guaranteed by aligning each of the basis vectors that span the latent space with a single factor. Each factor is specified as a set of weak labels over the high-dimensional space and thus for the same data the framework can learn different representations, given different sets of symbols. We test the framework both on a synthetic dataset (modified dSprites [9] with added color), with controlled factors of variation and on a dataset of real-world objects captured from a set of human demonstrations for the task of sorting table-top objects according to the user’s preference.

## 2 Related Work

An efficient, and unobtrusive, learning process must require minimal effort on the part of the human expert, requiring the agent to be able to generalise to unobserved scenarios. At the same time,

the models and concepts used by the agent must be interpretable by the human, in order for the interaction to be efficient. 0-shot, 1-shot [10] and meta-learning [11] are all approaches which strive for fast learning and better generalisation from limited amounts of data. However, from the point of view of ensuring safe operation by a robot, it is also important to be able to quantify when an unfamiliar situation occurs and to seek guidance from an expert.

The ability to deal with examples that fall outside the domain of the training distribution is known as ‘open world recognition’ [12, 13]. This is needed when an agent comes across *unknown unknowns* - observations that have not been seen during training. In this setting, the incomplete nature of the agent’s model causes it to make the wrong prediction. A complete model would cope with such cases by explicitly recognising that data point as ‘unknown’. It is desirable for the agent to be able to express its *ignorance* to the expert in a way that is comprehensible to them. This motivates the need for interpretability - we learn a representation that enables communication for user feedback regarding partially labelled sensory observations.

In the context of visual sensory inputs, ‘inverse graphics’ is an approach to learning compressed and factorised representations of high-dimensional visual data - e.g. learn to invert a graphical renderer and infer (for a given image) the parameter vector that generated an input image. The fact that such vectors are low-dimensional and factorised is what makes them appealing from a human-interpretability point of view [14, 15].

In the representation learning literature, there has been work [16, 17, 18, 19, 20] aimed at unsupervised learning of inverse graphics like representations of image datasets. Naturally, the factors of variation which end up being learnt are the ones that best explain the variations in the data— [21]—but this might not necessarily be the factors of variation which are crucial to recognise and discriminate in a particular task. Inferring which learnt factors best ground the user-defined symbols is usually a separate process wherein inference must be performed for each label-factor pair. However, simultaneously learning a representation suitable for symbol grounding from raw pixels in an unsupervised manner has turned out to be non-trivial [22]. In this work we employ methods based on deep variational inference [23] and perform the learning of a factorised vector space and the grounding of symbols in it simultaneously, in a weakly-supervised fashion. Thus we achieve better alignment between the user-defined semantic conceptual groups and the basis vectors of the vector space.

### 3 Background and Problem Formulation

In this work we assume that the human expert and robotic agent share the environment and can both observe and interact with objects in the surrounding world. The agent can extract images of distinct objects from the world and receive labels for them from the expert.

The data capture can be achieved with any technique that is able to align a sequential abstract plan for a task (parsed from a linguistic construct) with a temporal trace of expert movements and actions in the external environment - e.g. gesture recognition [24], movement tracking [25], eye-tracking [26]. Thus specific symbols from the plan can be related to regions of interest in the environment, where the object, encoding the label’s meaning, resides.

Let  $\mathcal{O} = \{\mathbf{x}_1, \dots, \mathbf{x}_N\}$ ,  $\mathbf{x}_i \in \mathbb{R}^D$  be a set of unlabelled observations, which have been passively gathered prior to the expert demonstration.

An expert demonstration introduces a set of  $L$  conceptual groups  $\mathcal{G} = \{g_1, \dots, g_L\}$  (e.g. color, shape, size, etc.), where each group is a set of mutually exclusive discrete labels:  $g_i = \{y_1^i, \dots, y_{n_i}^i\}$ ,  $n_i = |g_i|$  (e.g. color can be red, blue, yellow, etc.). The demonstration also provides labels, one drawn from each concept group, to  $M$  of the observations:  $\mathcal{O} = \{(\mathbf{x}_1, \mathbf{y}_1), \dots, (\mathbf{x}_M, \mathbf{y}_M), (\mathbf{x}_{M+1}, \emptyset) \dots (\mathbf{x}_N, \emptyset)\}$ ,  $\mathbf{y}_j = \{y^p\}$ ,  $p \in \{1, \dots, L\}$ ,  $y^p \in g_p$  is a set of labels which have been attached to the image  $\mathbf{x}$  - one per concept group.

The task is to project each  $\mathbf{x} \in \mathbb{R}^D$  into  $\mathbf{z} \in \mathbb{R}^C$ ,  $C \ll D$ , where the space of  $\mathbb{R}^C$  possesses the following properties:

**Axes Alignment** - guarantees a one-to-one mapping from the concept groups  $\mathcal{G}$ , to the orthogonal basis vectors which span  $\mathbb{R}^C$ . This would guarantee that independent concepts in image space are kept independent in  $\mathbb{R}^C$ —e.g. color does not depend on the size, orientation or shape of an object

and that should be represented in the feature space which is used to ground symbols like *blue*, *square* and *small*.

**Intra-group Linear Separability** - the latent clusters in  $\mathbb{R}^C$ , corresponding to the labels in each concept group  $g_i$ , are linearly separable across the basis vector which has been aligned to that concept group.

These two properties allow for  $\mathbb{R}^C$  to be used as a feature space for performing probabilistic symbol grounding with the ability to recognise *unknown* objects. For that we use KNN classification with 1D normal distributions (one per label) for each concept group in  $\mathcal{G}$ .

## 4 Methodology

We explore the effects of adding an auxiliary classification loss to a Variational Autoencoder [23] as a base architecture, specifically the  $\beta$ -VAE [16]. Through weak supervision, in the form of partially labelled data, the auxiliary loss influences the latent space of the model to possess properties which make it suitable for robust symbol classification. The model consists of a convolutional encoder network  $q_\phi$ , parametrised by  $\phi$ , a deconvolutional decoder network  $p_\theta$ , parametrised by  $\theta$ , and a set of linear classifiers parametrised by  $\mathbf{w}_i \in \mathbb{R}^{|g_i|}$  for each group  $g_i \in \mathcal{G}$ . Additional parameters— $\alpha, \beta, \gamma$ —are added on the three terms of the overall loss function—see (1)—in order to leverage their importance.

$$\min_{\theta, \phi, \mathbf{W}} \mathcal{L}(\mathbf{x}, \mathbf{y}, \theta, \phi) = \beta D_{KL}(q_\phi(\mathbf{z}|\mathbf{x})||p_\theta(\mathbf{z})) - \alpha \mathbb{E}_{q_\phi(\mathbf{z}|\mathbf{x})}(\log p_\theta(\mathbf{x}|\mathbf{z})) + \gamma \sum_g^G H(z_g W_g^T, \mathbf{y}_g) \quad (1)$$

**Classification term** (weighted by  $\gamma$ ) - In order to force the learnt latent space to explain the variations in the data, we add a linear classifier for each concept group. Each classifier has to predict the set of labels for its assigned concept group using information only from single latent dimension. No two classifiers have access to the same latent dimension. That forces each dimension to only explain labels from the particular concept group. A discrete cross-entropy term is used for the predictions of each classifier.

**Reconstruction term** (weighted by  $\alpha$ ) - The reconstruction loss is a standard Bernoulli Negative Log Likelihood, which is used to predict the pixel values across the three RGB channels. The motivation behind using it is the fact that we assume not all data points in our dataset are labelled. Thus the reconstruction loss would force data points which look similar in image space to be projected close to each other in the latent space.

**Kullback-Leibler divergence term** (weighted by  $\beta$ ) - The Kullback-Leibler divergence term ensures that the distribution of the latent projections of the data in  $\mathbb{R}^C$  does not diverge from a prior isotropic normal distribution. A perfectly optimised KL term would result in all latent projections to be 0. This forces the encoder network  $q_\phi$  to be more efficient when encoding the image observations so that their latent projection can be discriminated from each other across the basis vectors aligned with  $\mathcal{G}$ —the classification term—and the decoder network  $p_\theta$  can efficiently reconstruct them—the reconstruction term.

In order to account for data-generative factors of variation that might not be needed to encode the conceptual groups  $\mathcal{G}$  but are still essential for good reconstruction and stable training, we allow  $|\mathbb{R}^C| > |\mathcal{G}|$ . For example, spatial and rotational factors of variation would not contribute to explaining the semantics of concepts like shape and size but should still be accounted for in order for the subset of basis vectors in  $\mathbb{R}^C$  which are aligned with  $\mathcal{G}$  to encode only information which explain  $\mathcal{G}$ .

Algorithm 1 describes the core functionality of the framework. Initially we have a set of partially labelled observations, a set of conceptual groups with their labels, and a single untrained linear classifier for each group. In the training process, each observed image  $\mathbf{x}$  is passed through the network and its reconstruction  $\hat{\mathbf{x}} \sim p_\theta(\mathbf{x}|\mathbf{z}), \mathbf{z} \sim q_\phi(\mathbf{x})$  is fed to the loss  $\mathcal{L}$ . If the data point is labelled, a label is predicted for each conceptual group from the respective classifier. After training, we estimate the parameters of a 1D normal distribution for each label across the dimension which was responsible for predicting it during learning.

---

**Algorithm 1:** Model Learning with Weak Supervision

---

**Input:** observations  $\mathcal{O} = \{(\mathbf{x}_1, \mathbf{y}_1), \dots, (\mathbf{x}_M, \mathbf{y}_M), (\mathbf{x}_{M+1}, \emptyset) \dots (\mathbf{x}_N, \emptyset)\}$   
**Input:** conceptual groups  $\mathcal{G} = \{g_1, \dots, g_L\}$   
**Input:** linear classifiers  $\mathcal{W} = \{\mathbf{w}_i\}, i \in \{1, \dots, L\}$   
**Input:** Isotropic Normal Prior  $p(z) = \mathcal{N}(0, I)$   
**Output:** set of per-label estimated 1D normal distribution for each label in each conceptual group:  
 $K = \{\{\mathcal{N}(\mu_q^p, \sigma_q^p)\}, p \in \{1, \dots, L\}, q \in \{1, \dots, |g_p|\}$

```
1 while not converged do
2   for each  $(\mathbf{x}, \mathbf{y})$  in  $\mathcal{O}$  do
3      $\hat{\boldsymbol{\mu}}, \hat{\boldsymbol{\sigma}} \leftarrow \text{Encode}(\mathbf{x});$ 
4      $\hat{\mathbf{z}} \sim \mathcal{N}(\hat{\boldsymbol{\mu}}, \hat{\boldsymbol{\sigma}}I);$ 
5     if  $\mathbf{y} \neq \emptyset$  then
6       for each  $\mathbf{w}_i$  in  $\mathcal{W}$  do
7          $\hat{\mathbf{y}}^i \leftarrow z_i \mathbf{w}_i^T;$ 
8        $\hat{\mathbf{x}} \leftarrow \text{Decode}(\hat{\mathbf{z}});$ 
9       Use  $\hat{\mathbf{x}}, \hat{\mathbf{y}}, \hat{\boldsymbol{\mu}}$  and  $\hat{\boldsymbol{\sigma}}$  to compute  $\mathcal{L}$ —see (1);
10  for each  $g_i$  in  $\mathcal{G}$  do
11    for each  $y_j^i$  in  $g_i, j = |g_i|$  do
12       $\mathbf{f} \leftarrow \{(\mathbf{x}, \mathbf{y}) \in \mathcal{O} | y_j^i \in \mathbf{y}\};$ 
13       $\hat{\boldsymbol{\mu}}, \hat{\boldsymbol{\sigma}} \leftarrow \text{Encode}(\mathbf{f});$ 
14       $\hat{\mathbf{z}} \sim \mathcal{N}(\hat{\boldsymbol{\mu}}, \hat{\boldsymbol{\sigma}}I);$ 
15       $\mathcal{N}(\mu_j^i, \sigma_j^i) \leftarrow \text{fitNormal}(\hat{\mathbf{z}}_i);$ 
16      Add  $\mathcal{N}(\mu_j^i, \sigma_j^i)$  to  $K;$ 
```

---

When classification is performed at test time, the task is to predict a set of  $L$  labels  $\mathbf{y}$  for each image observation  $\mathbf{x}$ . Classification is performed by using the factored projecting of each image observation in  $\mathbb{R}^C$ . The 1 dimensional coordinates along each basis vector  $\mathbf{z}_i$  of  $\mathbb{R}^C$  are used to predict a label for the correspondingly aligned concept group  $g_i$ . Each 1D value is normalised with respect to the normal distributions in  $K$  corresponding to  $g_i$  and the class associated with the closest one, along  $\mathbf{z}_i$  is assigned to  $\mathbf{x}$  for  $g_i$ . As a consequence of optimising the Kullback-Leibler divergence term, together with the reconstruction and classification losses, any data points that have not been labelled and do not resemble the labelled ones end up being projected closer towards the origin of the latent space  $\mathbb{R}^C$ , in between the clusters associated with the labelled data. Thus, in order to be able to account for such unknown objects, for every two neighbouring distributions  $\mathcal{N}(\mu_r^i, \sigma_r^i)$  and  $\mathcal{N}(\mu_l^i, \sigma_l^i)$ , along the basis vector  $\mathbf{z}_i$ , aligned with  $g_i$  we fit an average distribution  $\mathcal{N}_u(\mu_u^i, \sigma_u^i)$  where  $\mu_u^i = \frac{\mu_l^i + \mu_r^i}{2}$  and  $\sigma_u^i = \frac{\sigma_l^i + \sigma_r^i}{2}$ . Any data point that is closer to such an *unknown* distribution than to a labelled one is considered *unknown*.

## 5 Experiments

### 5.1 Data

The controlled data-generative factors of variation of the modified dSprites dataset—see Figure 2—make it suitable for exploring how the two baselines compare to the proposed model with respect to the defined manifold properties in section 3. The resulting dataset is of size 3500 images—72 objects with spatial x/y variations in the image). We perform two experiments with the same underlying dataset but different sets of symbols in order to demonstrate how the user’s preference is encoded in the latent space.

In order to demonstrate the application of the framework to real-world human-robot interaction scenarios, a second dataset of 15 objects on a table-top is gathered from a human demonstration - Figure 3. The task the human performs is to separate the objects by their function - *juggling balls* vs *orbs*, and then by their color - *red* vs *yellow* vs *blue*. Lego blocks and whiteboard pins are also present in the scene, but they are not manipulated and no label information is given about them by the expert. At test time the agent has to repeat the task, with new objects being present in the scene

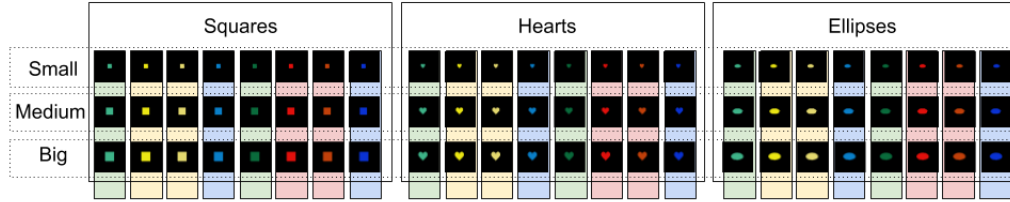


Figure 2: A modified version of the dSprites [9] dataset with added color. The RGB equivalents of 8 colors—two variations of red, green, blue and yellow—are added. Spatial factors of variation are also present in the images but not shown in the figure.

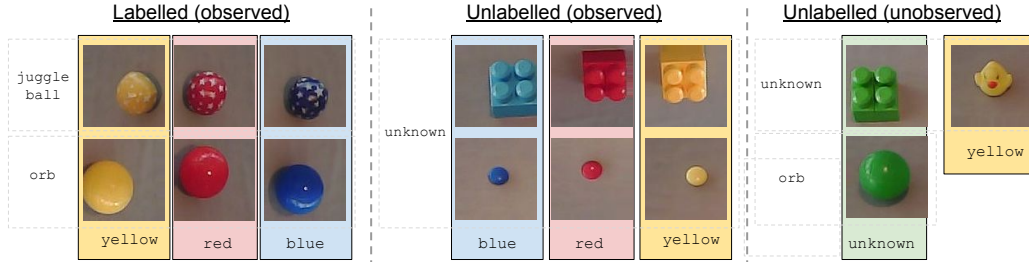


Figure 3: Example images crops of all table-top objects. Spatial and pixel noise factors of variation were added to each crop through data augmentation techniques.

that were previously unobserved—*green* objects and a *yellow rubber duck*. Each object image is augmented, resulting in a dataset of size 7500 images. The setup for gathering and labelling per-object image crops in a single human demonstration through the use of eye-tracking is described in Appendix A.

Both datasets are split into a training-testing sets with an 80-20 ratio. All results are reported on the test set.

## 5.2 Evaluation

**Baselines** - Two baselines were used to benchmark against the proposed architecture - a Vanilla Beta-VAE ( $\gamma = 0$ ) and a Convolutional Classifier Network with Kullback-Leibler divergence and no reconstruction term ( $\alpha = 0$ ). Across all experiments, for all three models, training was performed for a fixed number of 200 epochs using a batch size of 32 and the Adam optimizer [27].

In order to evaluate how much each baseline satisfies the properties we defined in Section 3 we use metrics which are inspired by the disentanglement learning community [28]

**Axes Alignment** - In order to determine how well the concept groups in  $\mathcal{G}$  are aligned with the basis vectors that span the latent space  $\mathbb{R}^C$  we perform PCA on the latent projections of the data points for each label and examine the orthogonality of the resultant eigenvectors with the basis vectors. If a particular concept group is explained by a single basis vector, then the eigenvector with the smallest eigenvalue should be parallel to that basis vector and orthogonal to all others. By "explain" we mean that traversing a single concept group in image space corresponds to perturbing the values a single basis vector. For example, if  $\mathbf{z}_i$  encodes the concept of *color*, then the latent distribution for all *blue* datapoints should have small variance across  $\mathbf{z}_i$  and big variance across all other  $\mathbf{z}_{j \neq i}$ . To examine this, for each label in each concept group we plot the cosine similarity diagrams depicting the cosine distance between each pair of basis and eigenvectors—see Figure 4. White cells mark the cosine similarities between the smallest eigenvector with all basis vectors and between its closest basis vector and all other principal components. The average entropy of the normalised white cosine values is reported for each pair of model-experiment. Low entropy satisfies axes alignment and would result in a single big white cell and remaining small white cells along the row and column of the big one.

**Intra-group Linear Separability** - In order to perform KNN classification at test time with unlabelled objects, using 1D Normal distributions across the concept groups in  $\mathcal{G}$ , the latent cluster in  $\mathbb{R}^C$  for each label  $y_j^i \in g_i$  has to be linearly separable from the latent clusters for all other labels from  $g_i$ . We report F1 scores for each class label, per concept group, including predictions for unlabelled observations which represent both known and unknown labels.

### 5.3 Results

**Experiment 1** - learn  $\mathbf{z}_1 \equiv \text{color}$  and  $\mathbf{z}_2 \equiv \text{size}$ . Latent dimension  $z_1$  is passed to the classifier for color and latent dimension  $z_2$  is passed to the classifier for size. The user-uttered labels for color are *red*, *blue* and for size are *small*, *big*. The color labels are assigned to a single variation of the respective color. All images which can not be described by the given labels—*yellow* and *green* for color and *medium* for size—are given an *unknown* ground truth label. Total  $|Z| = 4$ .

**Experiment 2** - learn  $\mathbf{z}_1 \equiv \text{shape}$  and  $\mathbf{z}_2 \equiv \text{size}$ . Latent dimension  $\mathbf{z}_1$  is passed to the classifier for shape and latent dimension  $\mathbf{z}_2$  is passed to the classifier for size. The user-uttered labels for shape are *square*, *heart* and for size are *small*, *big*. All images which can not be described by the user-uttered labels—*ellipse* for shape and *medium* for size—are given an *unknown* ground truth label.

**Experiment 3** learn  $\mathbf{z}_1 \equiv \text{color}$  and  $\mathbf{z}_2 \equiv \text{object type}$ . Latent dimension  $\mathbf{z}_1$  is passed to the classifier for color and latent dimension  $\mathbf{z}_2$  is passed to the classifier for object type. The user-uttered labels for color are *red*, *blue* and for object type are *juggle ball*, *orb*. All images which can not be described by the user-uttered labels—*lego bricks* and *whiteboard pins*, *rubber ducks* or *green objects*—are given an *unknown* ground truth label.

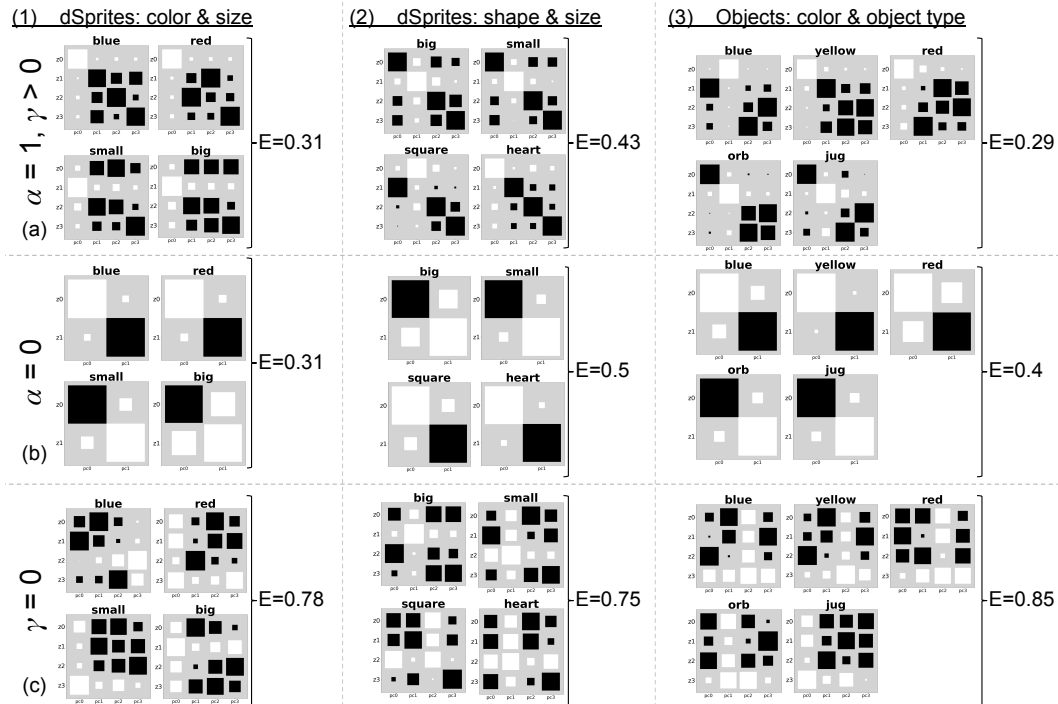


Figure 4: Axes Alignment evaluation for the full model (a), the classifier baseline (b) and the  $\beta$ -VAE (c) for the 3 experiments - (1), (2) and (3) respectively. For each experiment and each model, the cosine similarity diagram is shown for each label. Each similarity diagram consists of 4x4 squares, where the size of square (i,j) represents cosine distance between eigenvector  $c_i$  and basis vector  $z_j$  in  $\mathbb{R}^C$ , after performing PCA on the latent values for the corresponding label. In a single diagram all white cells mark the cosine similarities between the smallest eigenvector with all basis vectors and between its closest basis vector and all other principal components.  $E$  denotes the average entropy estimates over normalised white cells values for a single model and a single experiment.

Figure 4 presents the main findings from the conducted experiments. Both the full model and the classifier network - Figure 4 (a,b) achieve good alignment between the concept groups in  $\mathcal{G}$  and the basis vectors of  $\mathbb{R}^C$ . All labels from a particular concept group are consistently explained by the latent dimension which was used to predict them - e.g. color is explained by  $\mathbf{z}_1$  and size is explained by  $\mathbf{z}_2$  for experiment 1. For the classifier network - Figure 4 (b) we show only the first two latent dimensions which were used to perform the classification and thus contain information. The plain variational autoencoder - Figure 4 (c) fails to satisfy the axes alignment requirement - labels from the same concept groups are best explained by different basis vectors—e.g. color in experiments 1 and 2. This renders it incapable to perform well in the test-time KNN classification, for which the factors of variation in latent projections of the data have to be factorised - Table 1. The full model and the classification network baseline perform comparably well with respect to classifying labelled data points. However, the classifier-only baseline is not as good at discriminating between known and unknown objects - *unknown* columns in Tables 1a, 1b, 1c. We speculate that is a result of the model having access only to labelled images during training, unlike the weakly trained full mode. Thus it is not being able to pull together in the latent space both labelled and unlabelled similarly looking data points in image space and space away visually different data points in image space. We provide more detailed analysis in the supplementary materials <sup>1</sup>.

Model	<i>blue</i>	<i>red</i>	<i>unknown</i>	<i>big</i>	<i>small</i>	<i>unknown</i>
$\alpha = 1, \gamma \neq 0$	<b>0.88</b>	<b>0.98</b>	<b>0.87</b>	0.82	<b>0.93</b>	<b>0.64</b>
$\alpha = 0$	0.76	0.78	0.29	<b>0.84</b>	0.87	0.52
$\gamma = 0$	0.05	0.37	0.23	0.45	0.34	0.26

(a) dSprites -  $\mathbf{z}_1 \equiv$  color and  $\mathbf{z}_2 \equiv$  size

Model	<i>heart</i>	<i>square</i>	<i>unknown</i>	<i>big</i>	<i>small</i>	<i>unknown</i>
$\alpha = 1, \gamma \neq 0$	0.70	0.73	0.34	<b>0.71</b>	<b>0.83</b>	<b>0.6</b>
$\alpha = 0$	<b>0.97</b>	<b>0.8</b>	<b>0.67</b>	0.53	0.79	0.5
$\gamma = 0$	0.2	0.33	0.32	0.4	0.38	0.33

(b) dSprites -  $\mathbf{z}_1 \equiv$  shape and  $\mathbf{z}_2 \equiv$  size

Model	<i>blue</i>	<i>red</i>	<i>yellow</i>	<i>unknown</i>	<i>juggle ball</i>	<i>orb</i>	<i>unknown</i>
$\alpha = 1, \gamma \neq 0$	<b>0.75</b>	<b>0.87</b>	0.86	<b>0.95</b>	<b>0.8</b>	0.62	<b>0.81</b>
$\alpha = 0$	0.7	0.31	<b>0.89</b>	0.1	0.64	<b>0.64</b>	0.41
$\gamma = 0$	0.2	0.25	0.25	0.18	0.1	0.3	0.26

(c) Real objects -  $\mathbf{z}_1 \equiv$  color and  $\mathbf{z}_2 \equiv$  object type

Table 1: Evaluation of the discriminative abilities of each model for each experiment. F1 scores are reported for experiment 1 (a), experiment 2 (b) and experiment 3 (c).

## 6 Conclusion

We present a framework for grounded language acquisition where linguistically-defined semantic concepts from an expert, manifested in a high-dimensional image space, are mapped to a lower-dimensional learnt latent space. The resultant latent projections preserve any orthogonality between the user-defined concepts and are thus sufficient to perform robust—recognising unknown unknowns—and sample-efficient symbol inference both over images of computer-generated and real objects.

## Acknowledgments

This work is partly supported by ERC Grant 269427 (STAC), a Xerox University Affairs Committee grant, and grants EP/F500385/1 and BB/F529254/1 for the DTC in Neuroinformatics and Computational Neuroscience from the UK EPSRC, BBSRC, and the MRC.

<sup>1</sup><https://sites.google.com/view/interpretable-latent-spaces/>



## References

- [1] B. D. Argall, S. Chernova, M. Veloso, and B. Browning. A survey of robot learning from demonstration. *Robotics and autonomous systems*, 57(5):469–483, 2009.
- [2] S. Ross, G. Gordon, and D. Bagnell. A reduction of imitation learning and structured prediction to no-regret online learning. In *Proceedings of the fourteenth international conference on artificial intelligence and statistics*, pages 627–635, 2011.
- [3] S. Levine, C. Finn, T. Darrell, and P. Abbeel. End-to-end training of deep visuomotor policies. *The Journal of Machine Learning Research*, 17(1):1334–1373, 2016.
- [4] C. Finn and S. Levine. Deep visual foresight for planning robot motion. In *Robotics and Automation (ICRA), 2017 IEEE International Conference on*, pages 2786–2793. IEEE, 2017.
- [5] S. Gu, E. Holly, T. Lillicrap, and S. Levine. Deep reinforcement learning for robotic manipulation with asynchronous off-policy updates. In *Robotics and Automation (ICRA), 2017 IEEE International Conference on*, pages 3389–3396. IEEE, 2017.
- [6] H. H. Clark. Language use and language users. *Handbook of social psychology*, 1985.
- [7] DARPA. Broad agency announcement on explainable artificial intelligence (xai). *DARPA-BAA-16-53*, 2016.
- [8] S. Wachter, B. Mittelstadt, and L. Floridi. Transparent, explainable, and accountable ai for robotics. *Science Robotics*, 2(6), 2017.
- [9] L. Matthey, I. Higgins, D. Hassabis, and A. Lerchner. dsprites: Disentanglement testing sprites dataset. <https://github.com/deepmind/dsprites-dataset/>, 2017.
- [10] I. Goodfellow, Y. Bengio, and A. Courville. *Deep learning*. MIT press, 2016.
- [11] S. Thrun and L. Pratt. *Learning to learn*. Springer Science & Business Media, 2012.
- [12] A. Bendale and T. Boulton. Towards open world recognition. In *Proceedings of the IEEE Conference on Computer Vision and Pattern Recognition*, pages 1893–1902, 2015.
- [13] H. Lakkaraju, E. Kamar, R. Caruana, and E. Horvitz. Identifying unknown unknowns in the open world: Representations and policies for guided exploration. In *AAAI*, volume 1, page 2, 2017.
- [14] O. Li, H. Liu, C. Chen, and C. Rudin. Deep learning for case-based reasoning through prototypes: A neural network that explains its predictions. *arXiv preprint arXiv:1710.04806*, 2017.
- [15] T. D. Kulkarni, W. F. Whitney, P. Kohli, and J. Tenenbaum. Deep convolutional inverse graphics network. In *Advances in Neural Information Processing Systems*, pages 2539–2547, 2015.
- [16] I. Higgins, L. Matthey, A. Pal, C. Burgess, X. Glorot, M. Botvinick, S. Mohamed, and A. Lerchner. beta-vae: Learning basic visual concepts with a constrained variational framework. 2016.
- [17] X. Chen, Y. Duan, R. Houthoofd, J. Schulman, I. Sutskever, and P. Abbeel. Infogan: Interpretable representation learning by information maximizing generative adversarial nets. In *Advances in Neural Information Processing Systems*, pages 2172–2180, 2016.
- [18] T. Q. Chen, X. Li, R. Grosse, and D. Duvenaud. Isolating sources of disentanglement in variational autoencoders. *arXiv preprint arXiv:1802.04942*, 2018.
- [19] S. Ainsworth, N. Foti, A. K. Lee, and E. Fox. Interpretable vaes for nonlinear group factor analysis. *arXiv preprint arXiv:1802.06765*, 2018.
- [20] E. L. Denton et al. Unsupervised learning of disentangled representations from video. In *Advances in Neural Information Processing Systems*, pages 4417–4426, 2017.
- [21] C. P. Burgess, I. Higgins, A. Pal, L. Matthey, N. Watters, G. Desjardins, and A. Lerchner. Understanding disentangling in beta-vae. *arXiv preprint arXiv:1804.03599*, 2018.

- [22] I. Higgins, N. Sonnerat, L. Matthey, A. Pal, C. P. Burgess, M. Botvinick, D. Hassabis, and A. Lerchner. Scan: learning abstract hierarchical compositional visual concepts. *arXiv preprint arXiv:1707.03389*, 2017.
- [23] D. P. Kingma and M. Welling. Auto-encoding variational bayes. *arXiv preprint arXiv:1312.6114*, 2013.
- [24] M. Eldon, D. Whitney, and S. Tellex. Interpreting multimodal referring expressions in real time. In *International Conference on Robotics and Automation*, 2016.
- [25] M. Al-Omari, P. Duckworth, D. C. Hogg, and A. G. Cohn. Natural language acquisition and grounding for embodied robotic systems. In *AAAI*, pages 4349–4356, 2017.
- [26] S. Penkov, A. Bordallo, and S. Ramamoorthy. Physical symbol grounding and instance learning through demonstration and eye tracking. In *Robotics and Automation, 2017 IEEE International Conference on*, Singapore, June 2017.
- [27] D. P. Kingma and J. Ba. Adam: A method for stochastic optimization. *arXiv preprint arXiv:1412.6980*, 2014.
- [28] C. Eastwood and C. K. Williams. A framework for the quantitative evaluation of disentangled representations. In *International Conference on Learning Representations*, 2018.
- [29] S. Oepen, D. Flickinger, K. Toutanova, and C. D. Manning. *Research on Language and Computation*, 2(4):575–596, 2004.
- [30] D. Flickinger, E. M. Bender, and S. Oepen. ERG semantic documentation, 2014. URL <http://www.delph-in.net/esd>. Accessed on 2017-06-15.
- [31] Pupil labs. URL <https://pupil-labs.com/pupil/>. Accessed on 2017-06-15.

# Appendices

## A Demonstration and Object Crops Gathering

To capture the objects dataset with a single demonstration from a human we employ the pipeline depicted in Figure 5 - the plan for the task is given in a natural language form which is deterministically parsed to an abstract sequential form of the type (action target location), where action corresponds to an element from a predefined set  $\mathcal{A}$ , target corresponds to a list of terms that describe an object in the world and location corresponds to a single symbol denoting a physical location in the environment. The narration of the plan execution by the human comprises one sentence per abstract instruction. Therefore, given a plan description, our semantic parser finds a mapping from each sentence to a corresponding instruction as defined by our abstract plan language. Elementary Dependency Structures (EDS) [29], which are output by parsing the sentence with the wide-coverage English Resource Grammar [30], are used as an intermediate step in this mapping procedure.

The demonstration is executed by the expert and their gaze fixations over the table surface are recorded for the duration of the demonstration at a rate of approximately 60Hz. The Pupil Labs eye tracking headset [31] is used. Post demonstration, the temporal alignment between the eye-tracking trace and the abstract sequential plan is performed using the GLIDE framework [26]. For each fixation that is aligned to a particular instruction, a 100x100 pixel image, centered at the fixation, is cropped from the worldview camera of the headset. The target labels from the instruction are attached to all corresponding crops.

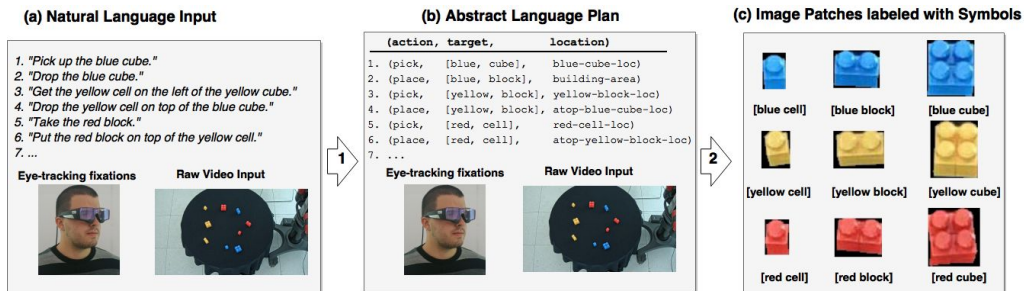


Figure 5: Overview of the dataset capturing pipeline for an example task. Input to the system are natural language instructions, together with eye-tracking fixations and a camera view of the world from above (a) Natural language instructions are deterministically parsed to an abstract plan language (b) Using the abstract plan, a set of labelled image patches is produced from the eye-tracking and video data (c)